13th World Conference on Earthquake Engineering
Vancouver, B.C., Canada
August 1-6, 2004
Paper No. 454

AMPLIFICATION CHARACTERISTICS OF K-NET, KIK-NET, AND JMA SHINDOKEI NETWORK SITES BASED ON THE SPECTRAL INVERSION TECHNIQUE

Hiroshi KAWASE [1] and Hidenori MATSUO [2]

SUMMARY

To predict strong ground motions for future scenario earthquake in a broad-band frequency range, we need to characterize both source spectra and site amplification. In this study we first try to separate the so-called source spectra, attenuation coefficient, and site amplification factors from K-Net, KiK-net, and JMA records observed throughout Japan. As a reference site we use one rock station of KiK-net. Once we obtain site amplification factors, we try to reproduce them by using one-dimensional S-wave velocity structures below each site. We succeed to reproduce site amplification factors at about one thirds of the sites very well. We then find how to explain site factors as a function of averaged S-wave velocities.

INTRODUCTION

To predict strong ground motions for future scenario earthquake in a broad-band frequency range, we need to characterize both source spectra and site amplification as precise as possible. For short period component we can use statistical method based on the observed records and the summation technique, that is, the statistical Green's function method [1]. Thanks to the advent of the K-Net and KiK-net in Japan, we have now plenty of weak motion data, enough to construct statistical Green's functions. On the other hand, in order to represent long- and intermediate period nature of the strong ground motion in the near field region, including both the forward rupture directivity effects and the basin effects, we need to use theoretical technique such as three-dimensional (3-D) finite difference method [2][3]. Theoretical methods need S-wave velocity structures that should reproduce the observed site amplification. It is desirable to have S-wave velocity explorations around a target site, but that would not be always the case. Thus we may use 1-D velocity profiles at the observed sites as a starting model to construct a more detailed 2-D/3-D basin model.

In this study we first try to separate the so-called source spectra, attenuation coefficient, and the site amplification factors from K-Net, KiK-Net, and JMA Shindokei network records observed throughout Japan. The separation method is the well-established one of Andrews [4] and the resultant source spectra

[1] Professor, Kyushu University, Fukuoka, Japan, Email: kawase@arch.kyushu-u.ac.jp
[2] Engineer, Hitachi System & Service, Tokyo, Japan, Email: hi-matsuo@hitachi-system.co.jp

are modeled as omega-square spectra. As a reference site we use one rock station of KiK-Net in Yamaguchi Prefecture, from which we remove the effects of shallow surface deposits. Once we obtain site amplification factors, we try to invert S-wave velocity structures below each site by assuming 1-D wave propagation theory. We then calculate averaged S-wave velocities over certain depths as representative values of site effects and see correlation for different depth averages with the spectral amplifications at different frequencies.

A REFERENCE SITE

In a simple spectral inversion method we need one additional constraint for separation of source, path, and site factors. There are many variations but physically speaking the simplest constraint is to take one station as a reference site. This means that this reference site has no amplification and the resultant source and site factors will be relative ones to this reference site. If there is some site effect at this site, then the deviation from true reference will be mapped onto all the source and site factors in an opposite (i.e., canceling-each-other) manner. Thus the success of the separation solely depends on the good choice of the reference site. Thanks to the wide range of site selection in KiK-net and its borehole station deployment, we can find several good candidates for a reference site among about 500 KiK-net sites. After the preliminary analysis of the spectral inversion, we search the best site for reference based on the separated site amplification factors, S-wave velocity of the borehole logging (open to the public at http://www.kik.bosai.go.jp/kik/index_en.shtml), and numbers of observed data. We choose YMGH01 because it has very high S-wave velocity layers below, as shown in Fig.1, and quite a small site effect. We also have sufficient numbers of strong motion records here. At the site we have a borehole sensor 200 m below the surface.

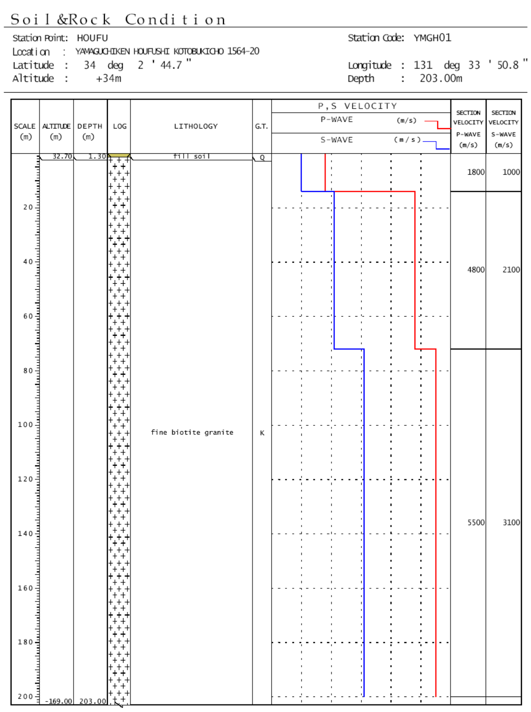

Fig.1 Soil profile at YMGH01 KiK-net site

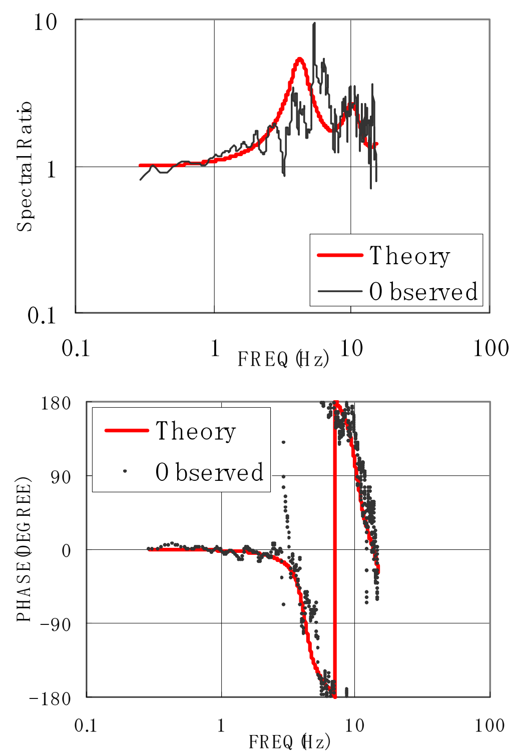

Fig.2 Amplitude and phase comparison at YMGH01

Although this is a site with rock outcrop, we have two weathered layers as seen in Fig.1. Since the amplification due to these weathered layers near the surface is small but not negligible, it would be better to remove the amplification by them. Before removing amplification based on 1-D wave propagation theory we invert the S-wave velocity structure for the optimal result through the so-called "Genetic Algorithm" using the amplitude and phase of the transfer function between borehole (-200m) and surface sensors. Fig.2 shows matching in amplitude and phase of the averaged transfer functions of observed data with 1-D theory. We found that the S-wave velocity of the basement rock reaches 3.4 km/sec as shown in Fig.3. The observed spectra at this reference site are corrected by using theoretical amplification from the outcrop of 3.4 km/sec layer to the surface, which is shown in Fig.4.

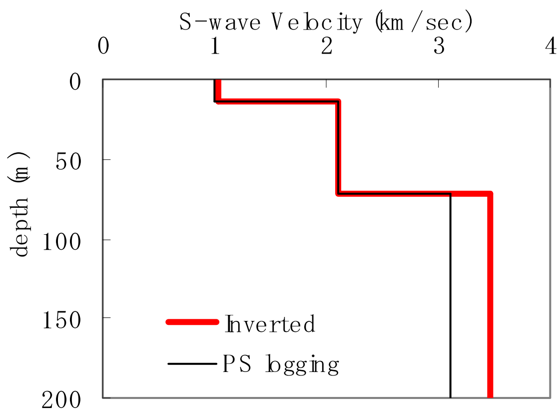

Fig.3 Original and inverted S-wave velocity profiles

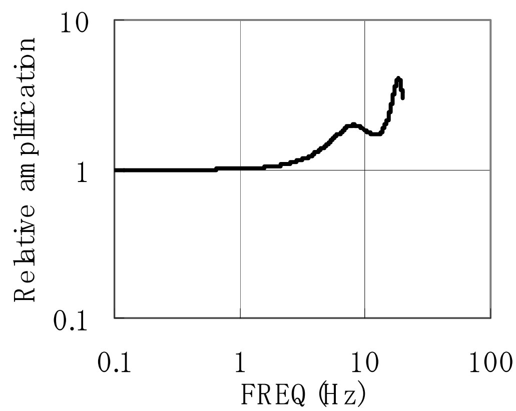

Fig.4 Amplification used to correct YMGH01

DATA AND METHOD OF ANALYSIS

Data source and data selection

We use here jointly K-NET, KiK-net, and JMA Shindokei network as a source of weak motions in Japan. K-NET started to operate from May 1996 with 1,000 surface stations, while KiK-net did from June 1997 with about 500 surface and downhole stations (at present 660 stations). K-NET stations have P-S logging velocity profiles up to 20 m (http://www.k-net.bosai.go.jp/), while KiK-net stations have those up to the depth of downhole stations, usually 100 m to 200 m (except for 21 sites inside sedimentary basins for which we have more than 1,000 m). We also use weak motion data from the JMA Shindokei network, which was designed to quickly broadcast JMA seismic intensity, Ijma and started to operate from October, 1996. Unfortunately JMA stations do not have any information on their site conditions, yet.

We collect not so strong and weak motion records observed by these three strong motion network from August 1996 to June 2002. Criteria to select appropriate earthquakes and data are: i) Mjma≧4.5, ii) depth ≦60km, iii) hypocentral distances X≦200km, iv) PGA≦200Gals, v) triggered station≧3 par earthquake, and vi) earthquakes ≧3 par site. By selecting observed records in this way final sites for inversion that can be connected by at least one common earthquake are 1,700 in total, 913 from K-NET, 468 from KiK-net, and 319 from JMA network and final earthquakes used are 228. Total numbers of source-station pairs are 15,800. We can divide these 228 earthquakes into three categories, namely, plate boundary earthquake B (99), intraplate (slab) earthquake I (81), and inland crustal earthquakes C (48). We show locations and mechanisms of the target earthquakes in Figs. 5 to 7.

Separation method and regions with different attenuation

First we cut out the target accelerograms from the onset of S-wave with the duration of 5 seconds (M<6), 10 seconds (M<7), or 15 seconds (M>7). Then we calculate Fourier spectra of these accelerograms. For

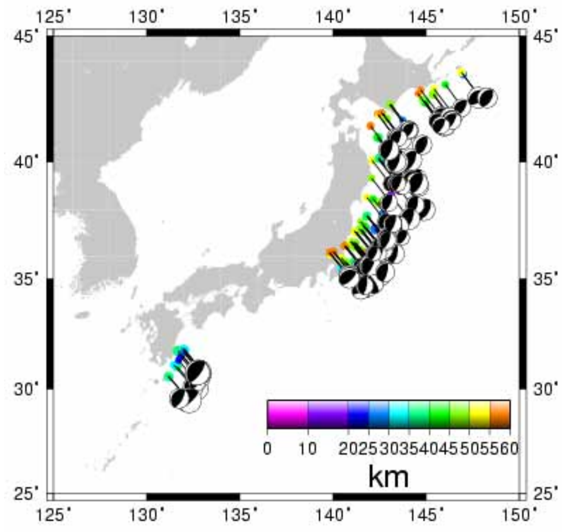

Fig. 5 Locations of plate boundary earthquakes

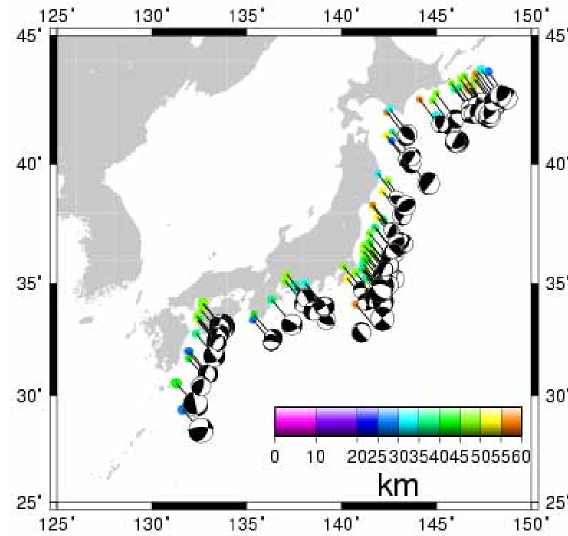

Fig. 6 Locations of intraplate earthquakes

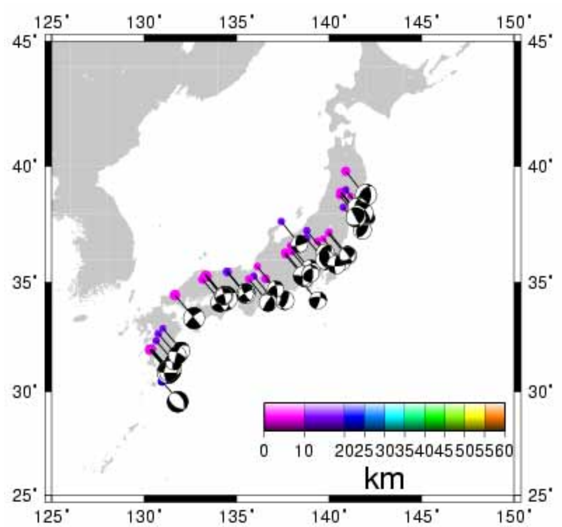

Fig.7 Locations of crustal earthquakes

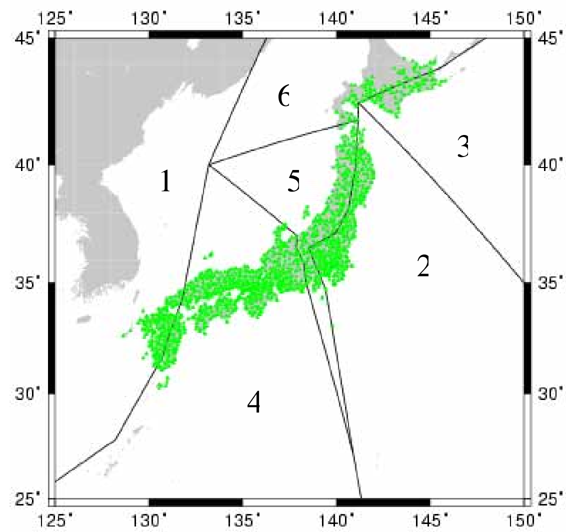

Fig.8 Regions for different attenuation factors

Fourier spectra *Fij* for i-th earthquake observed at j-th site we use the following equation:

$$\log F_{ij} = \log S_i - n_{l(i)} \log X_{ij} + \sum_k b_{l(i)k} X_{ijk} + \log G_j \tag{1}$$

$$X_{ij} = \sum_k X_{ijk} \tag{2}$$

where, *Si* is the source spectrum for i-th earthquake, *Gj* is the site factor for j-th site, *Xij* is the hypocentral distance for that pair, k is a region number with different attenuation, *l(i)* is a source type (B, I, or C). We use both parameters for geometrical spreading n and intrinsic and scattering attenuation b. To delineate different attenuation characteristics at different regions in Japan, we divide Japan into six regions, as shown in Fig.8, in which we assume different attenuation coefficient b. We also assume that these parameters n and b are source type dependent. The reason why we introduce n as a parameter for separation is to explain small attenuation in the intermediate distance range for shallow crustal earthquakes. We assume constant n equal to 1 for distance from 0 to 100 km.

ATTENUATION CHARACTERISTICS

First of all we present the result of attenuation determined by the spectral inversion. In Figs. 9 to 11 we show 1/Q values translated from attenuation coefficients b using equation (3) below and geometrical spreading factors n for different distance ranges and different source types.

$$1/Q(f) = \frac{-b(f) \cdot Vs \cdot \ln 10}{\pi \cdot f} \tag{3}$$

Here we assume Vs=4.0km/sec for plate boundary and intraplate earthquakes and Vs=3.6km/sec for crustal earthquakes. It is clear that 1/Q in the back-arc regions of Japan islands, namely regions 1 and 5, are high and that geometrical spreading factors are equal to 1 except for low frequency range of crustal earthquakes. Detailed inspection shows that the region 5 does not show so large 1/Q values for intraplate and crustal earthquakes. This suggests that low Q zones due to volcanic activity in northeastern Japan should have limited volume, as seen in the 3-D Q inversion study by Nakamura and Uetake [5]. For crustal earthquakes geometrical spreading factors become smaller as frequency goes lower or distance goes larger. This phenomenon may reflect the effects of Moho and Conrad reflection and some

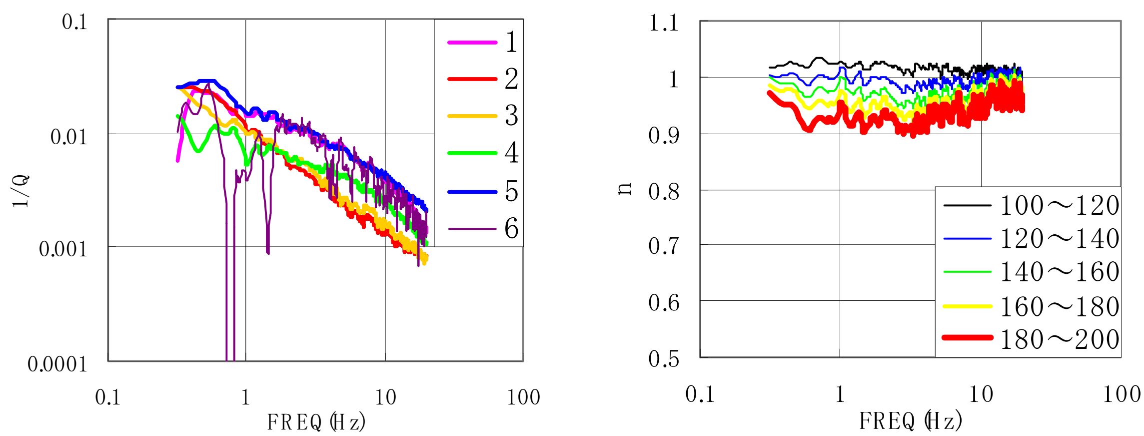

Fig. 9 Attenuation parameters, 1/Q and geometrical spreading factor, for plate boundary earthquakes

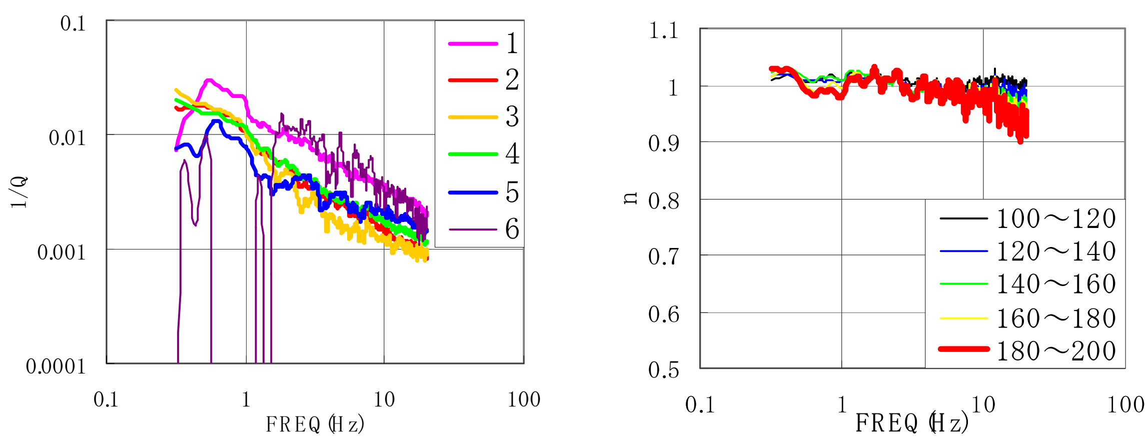

Fig. 10 Attenuation parameters, 1/Q and geometrical spreading factor, for intraplate earthquakes

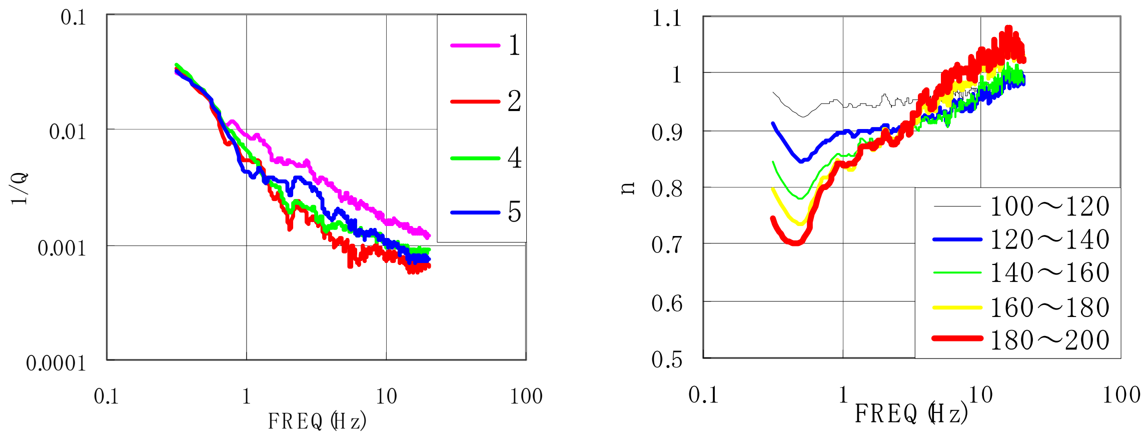

Fig. 11 Attenuation parameters, 1/Q and geometrical spreading factor, for crustal earthquakes

contamination of surface waves. Note that 1/Q is unstable in the lower frequency range for region 6 because not enough data and traveling distance exist. Also we cannot determine 1/Q of crustal earthquakes for regions 3 and 6 because we do not have sources in these regions (Hokkaido) as shown in Fig.7.

SOURCE SPECTRA AND ITS PARAMETRIZATION

Next we analyze source characteristics determined by the inversion. We translate source factors into moment density function by using the following equation:

$$M(f) = \frac{4\pi\rho Vs^3 S(f)}{\omega^2 R_{\theta\varphi} Fs P_R} \tag{4}$$

where,

- $M(f)$: moment density function (10^{-7} N・m)
- ρ: density (g/cm^3)
- Vs: S-wave velocity (km/s)
- $R_{\theta\varphi}$: radiation coefficient
- Fs: free-surface effect
- P_R: energy distribution coefficient into two components.

For plate boundary and intraplate earthquakes we use ρ=3.0g/cm^3 and Vs=4.0km/sec, while for crustal earthquakes ρ=2.7g/cm^3, Vs=3.6km/sec. We also assumes $R_{\theta\varphi}$ to be 0.63, Fs=2.0, and $P_R=1/\sqrt{2}$. Then by applying ω^{-2} model with a corner frequency fc and a cut-off frequency fmax to the obtained moment density functions, we can determine fc and fmax using a grid search method. We use the seismic moment determined by the broadband seismometer network, F-net [6]. As shown in Fig. 12 we can fit modeled source spectra to observed spectra very well.

We then calculate stress drops of Brune [7] from fc and compare them for different type earthquakes. We restrict the sources with the JMA magnitude larger than 5 because of uncertainty in seismic moment estimate for smaller earthquakes. Figs. 13 to 15 show stress drops as a function of seismic moment and as a function of source depth. As for plate boundary earthquakes the average stress drop is about 100 bars and log-standard deviation is about twice. Depth dependency is quite small, although the maximum stress drop level for a certain depth seems to exist. Note that sources in Hyuganada, near Kyushu, which are

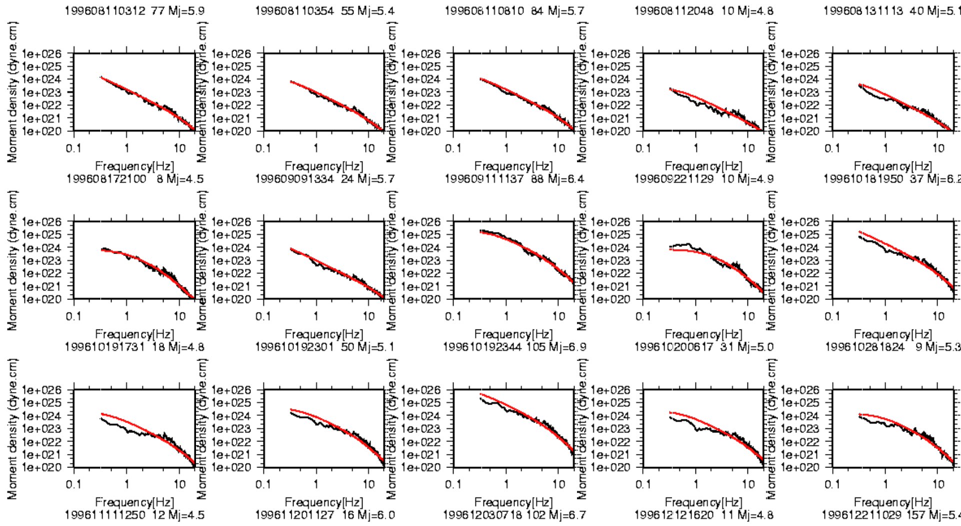

Fig. 12 Examples of matching between observed source spectra and modeled source spectra

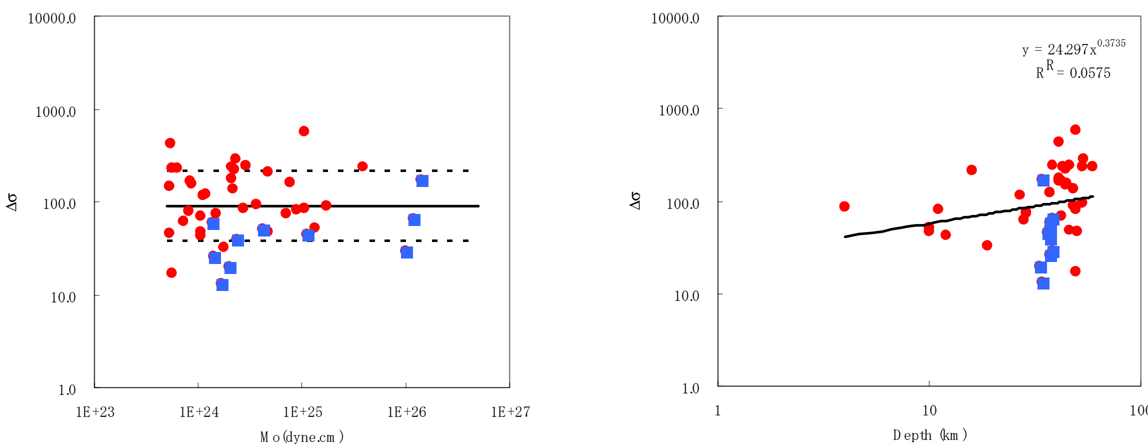

Fig. 13 Brune's stress drops as a function of M_0 and depth for plate boundary earthquakes

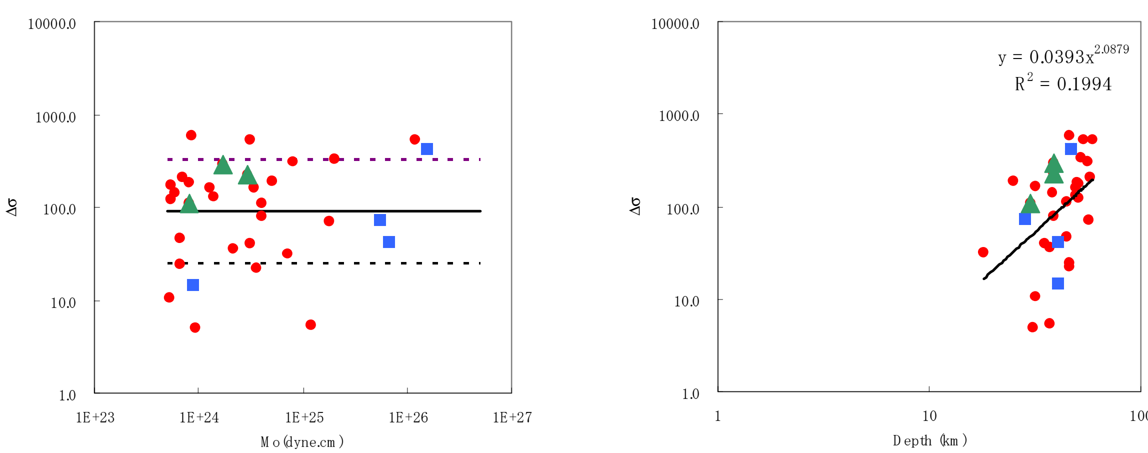

Fig. 14 Brune's stress drops as a function of M_0 and depth for intraplate earthquakes

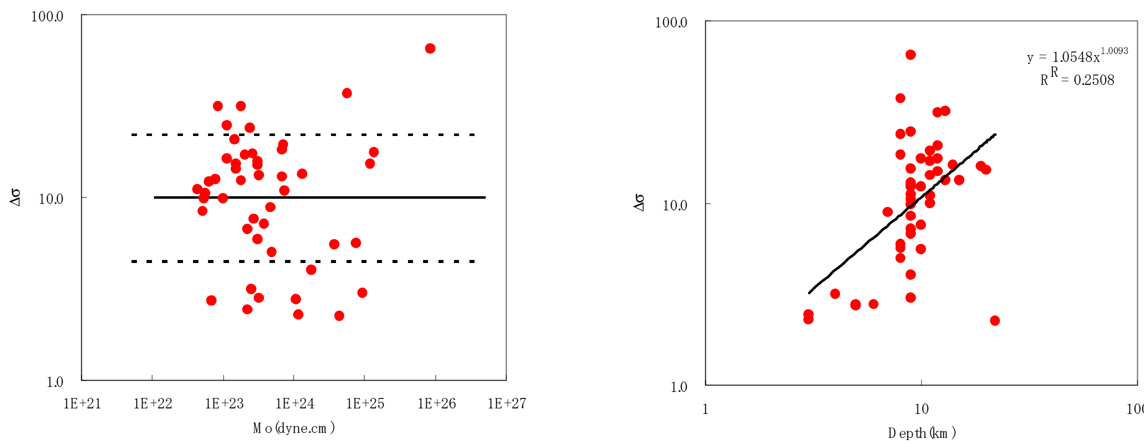

Fig. 15 Brune's stress drops as a function of M_0 and depth for intraplate earthquakes

shown by different symbols (solid squares), have systematically smaller stress drops. As for intraplate earthquakes we have the similar average value, about 100 bars with a larger deviation, about 3 times. No systematic difference is found for sources on the Philippine Sea Plate (solid squares and triangles). We can see clear depth dependence for intraplate earthquakes, although its linearity (hence correlation) is not so high. As for crustal earthquakes we found only 1/10 of the average stress drop, that is, about 10 bars. The coefficient of variation for crustal earthquake is about 2.2. We see some kind of depth dependence, that is, there seem to exist a certain threshold depth for high stress drop. Anyway the relationship is not linear at all. Basically for all the three types of earthquake we see no clear dependence of stress drop on the seismic moment. However, we can see some increasing tendency of stress drop for earthquakes larger than 1.0×10^{25} dyn.cm, especially for crustal earthquakes. The stress drop of the largest crustal event in our database, that is, the 1999 Tottori-ken Seibu earthquake of Mjma 7.3, shows the largest value of 64 bars. Fig.15 shows we may need to correct stress drop difference between the target main shock of M>7 and small earthquakes used for statistical Green's function.

SITE AMPLIFICATION FACTORS

We have obtained site amplification factors at 1,700 points throughout Japan with variety of soil conditions. We only show a few examples of separated site amplifications here. Fig. 16 shows observed

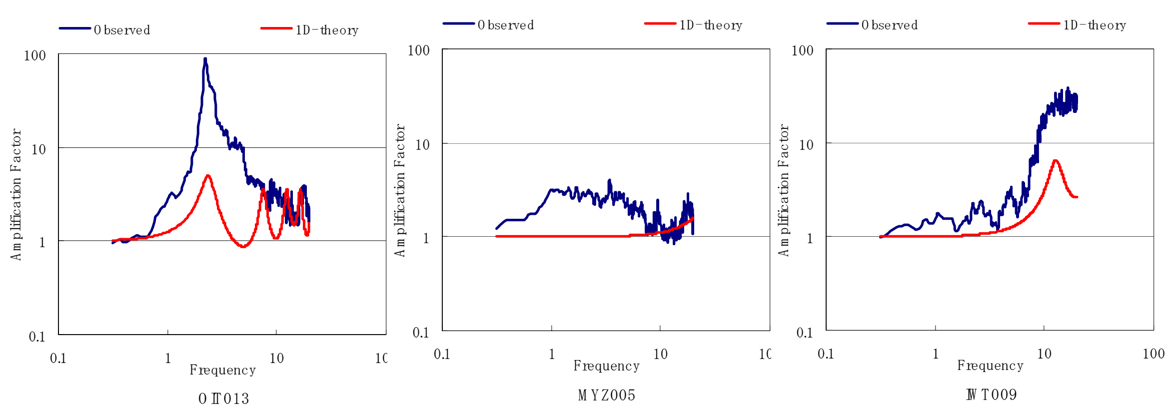

Fig. 16 Amplification factors separated from records observed at three K-NET sites

site amplification factors relative to the reference site, i.e., the outcrop of rock with Vs=3.4 km/sec at three representative K-NET sites. Red lines show theoretical 1-D amplification factors of soil layers based solely on the soil profiles up to 20 m. At OIT013 we have a very predominant peak of about 90 at 2.2 Hz, which corresponds to the theoretical predominant peak of shallow sediments. The difference between this theoretical peak level and the observed one should be attributed to first the impedance difference between the rock outcrop at the reference site and the bottom layer of the assumed K-NET velocity profile and to the local topographic effects near the site. MYZ005 has a Vs=1,070 m/sec rock formation 4 m below the surface so the amplification remains less than 3 for most of frequencies. IWT009 has also a hard rock formation with Vs=950 m/sec 6 m below but shallow deposits are relatively soft so that we have large amplification from 15 to 20 Hz. Since PS logging data provided for K-NET and KiK-net are not sufficient to explain observed site amplifications because of their truncated depths. Thus we invert the S-wave velocities of layers between the bottommost layer of PS logging and the reference bedrock with Vs=3.4 km/sec.

1-D SOIL LAYERS INVERTED FROM SITE FACTORS

We obtained site amplification factors for all the 1,700 sites. Since our reference site is a hypothesized rock outcrop with Vs=3.4 km/sec, we can consider them absolute site factors from the seismological bedrock. We try to construct 1-D S-wave velocity structures from the b=3.4 km/sec basement to the bottom of PS logging data. We fix PS logging data and invert only three layers' parameters (i.e., thickness and Vs) plus the thickness of the bottommost layer to minimize the residual between observed site effects and theoretical amplification factors from 0.3Hz to 20Hz. We again use genetic algorithm for the inversion. We exclude all the JMA stations since we do not have PS logging data at these sites. The density of each layer is calculated as a function of S-wave velocity as follows:

$$\rho_i = 1.4 + 0.67\sqrt{Vs_i} \tag{5}$$

We assume the same Q of $19f^{0.52}$ for all the layers to avoid the trade-off between Vs and damping. Fig. 17

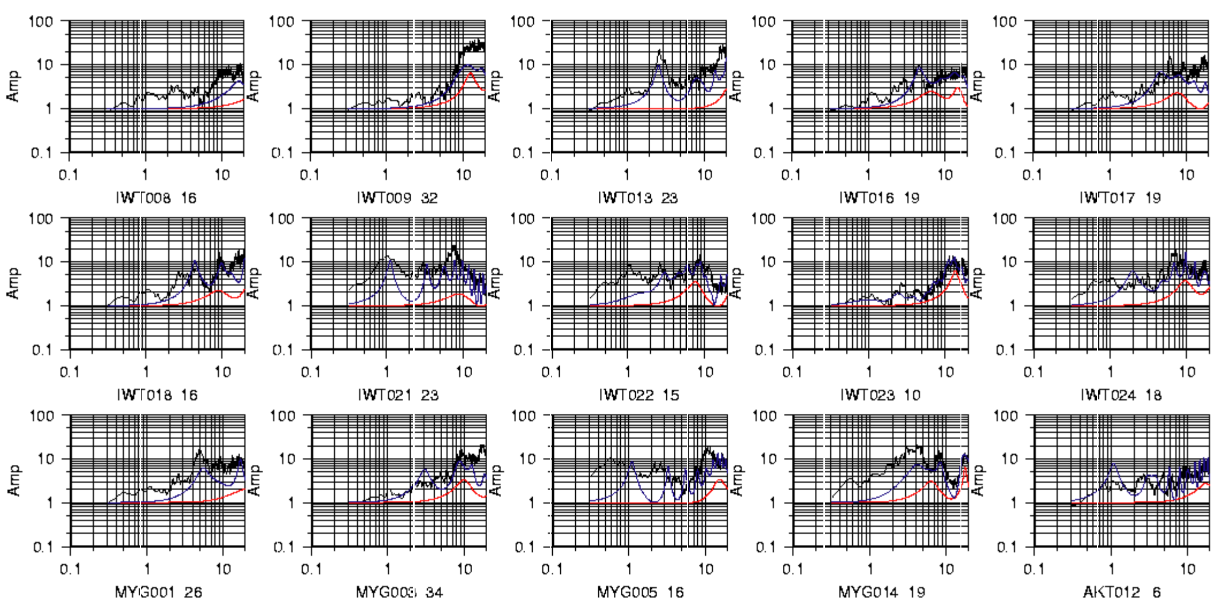

Fig. 17 Examples of matching between observed site factors and inverted 1-D soil amplification

shows comparisons of theoretical 1-D amplification with inverted site factors. Red lines show 1-D amplification only for the PS logging layers, while blue lines show those inverted by GA. We can reproduce quite well the observed site factors at about 1/3 of the 1,300 K-NET and KiK-net sites.

We need to define quantitative criteria to distinguish well reproduced sites from the others so that we can perform further analyses only for sites with reliable velocity profiles. After several trials we decide to use both the total residuals σ and the correlation coefficients ζ between theory and observation. We select 404 sites using the condition σ< 0.4 and ζ >0.5 as shown in Fig.18. Now we have 404 sites with S-wave velocity profiles from the surface to the seismological bedrock and site amplification factors.

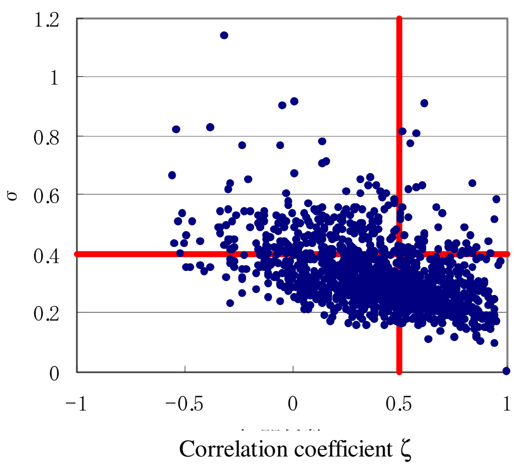

Fig. 18 Distribution map of total residual and correlation coefficient for all the 1,300 sites

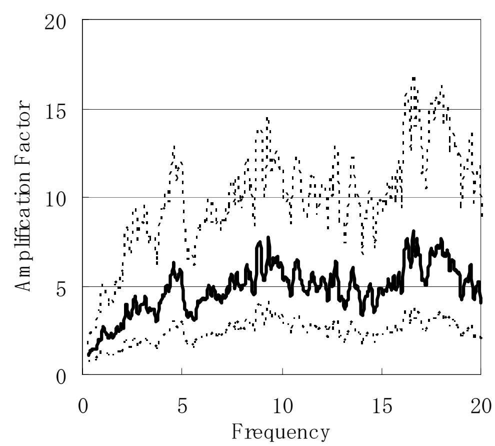

Fig.19 Averaged amplification factors for 404 good sites

SITE AMPLIFICATION AND AVERAGED VELOCITY

It is desirable if we can predict site amplification based on some kind of site categories or a certain site index such as averaged S-wave velocity. We see the difference of spectral site amplification factors as a function of averaged S-wave velocities. Fig. 19 shows the average and average plus/minus one standard deviation amplification factors for all the 404 good sites. We have about 5 times amplification at about 5

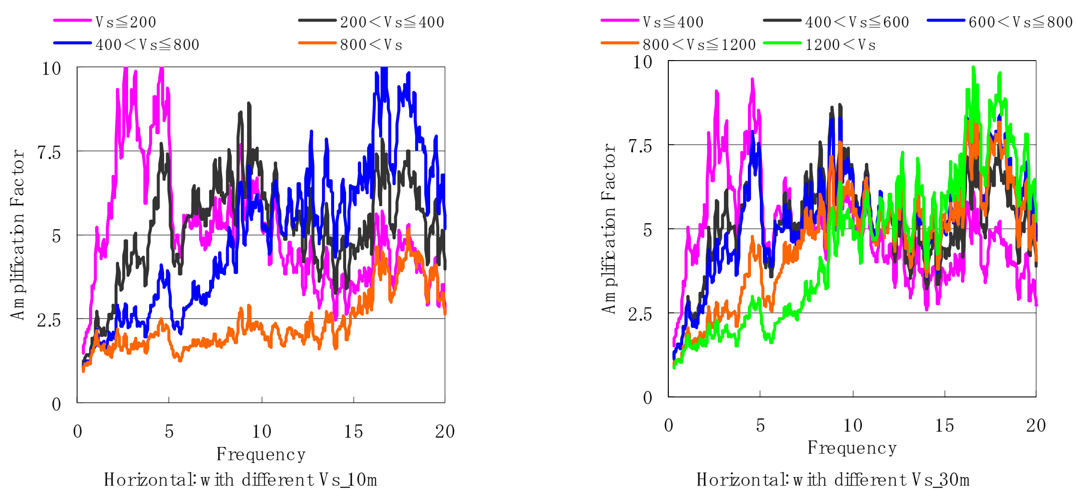

Fig. 20 Site amplification factors averaged for sites with different averaged S-wave velocities

Hz. Then we have almost flat amplification till 20 Hz. The coefficient of variation is about twice for all the frequencies. When we look at the amplification factors averaged over certain averaged Vs ranges, we see different characteristics as shown in Fig.20. The panel in the left-hand side shows those for S-wave velocities averaged over 10 m below the surface, Vs_10m, and the panel in the right-hand side shows those for velocities averaged over 30 m below the surface, Vs_30m. The latter has been used frequently to estimate site amplification by using empirical relationships [8][9]. As you can see in the left panel, the averaged site amplification factors show systematic difference if categorized for Vs_10m. Sites with low Vs_10m shows high amplification in a low frequency range, while sites with high Vs_10m show significantly smaller amplification in a low frequency range but some amplification in a high frequency range. The same observations can be made for the case of Vs_30m in the right panel, however, the separation of characteristics between different Vs_30m categories is not as clear as that between Vs_10m categories. The numbers of site for each category of Vs_10m or Vs_30m is dominant in the range of 200 to 400 m/sec for Vs_10m and in the range of 400 to 800 m/sec for Vs_30m. Thus the averaged site amplification characteristics for these Vs ranges are similar to the averaged site amplification for all the sites in Fig. 19.

Next we check the correlation between the averaged S-wave velocities and spectral amplification factors. Fig. 21 shows scatter diagrams for 1/3 Octave band average of site factors (the central frequencies are 2.0 Hz, 3.15 Hz, and 5 Hz) as a function of Vs_10m. Fig. 22 is the same figure for Vs_30m. Linear regression lines are shown in each panel. As you can see Vs_10m shows the same or better correlation with site amplification factors in these frequency ranges than Vs_30m.

We can see the summary of correlation coefficients between site factors averaged over certain frequency ranges and Vs averaged over certain depths, as shown in Fig. 23. It shows that the higher the frequency range of interest is the shallower the necessary depth for average. This is quite physical since high fre-

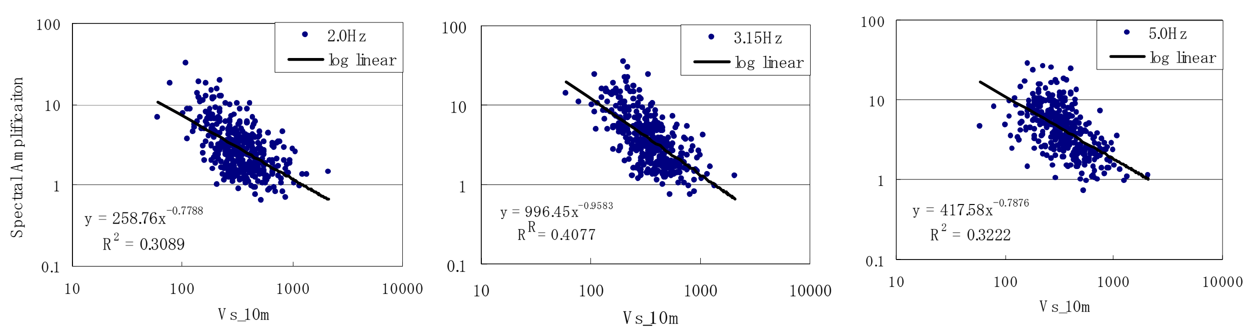

Fig. 21 Relationship between Vs_10m and site factors averaged over 1/3 octave band

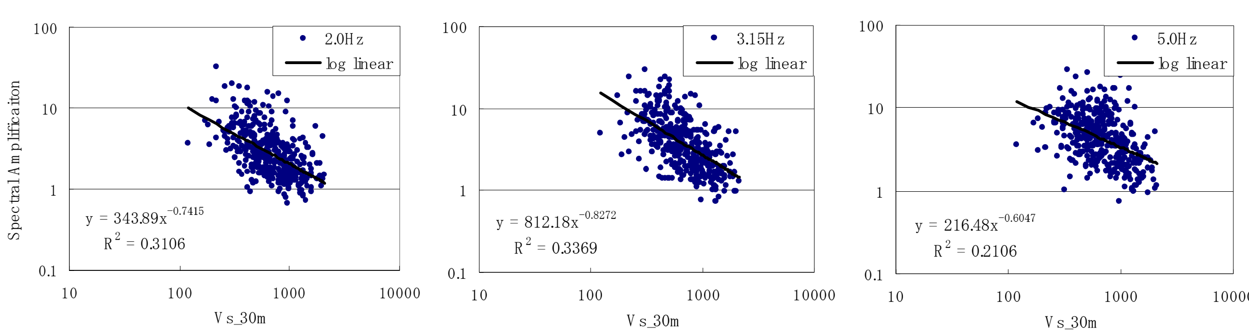

Fig. 22 Relationship between Vs_30m and site factors averaged over 1/3 octave band

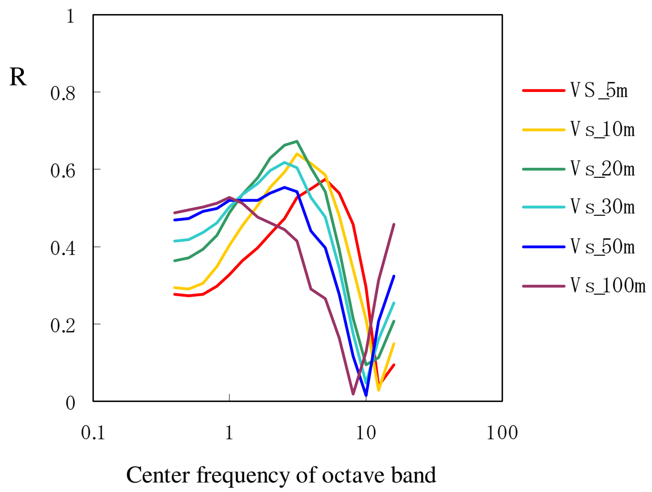

Fig. 23 Correlation coefficients for different frequency ranges using different average depths of layers

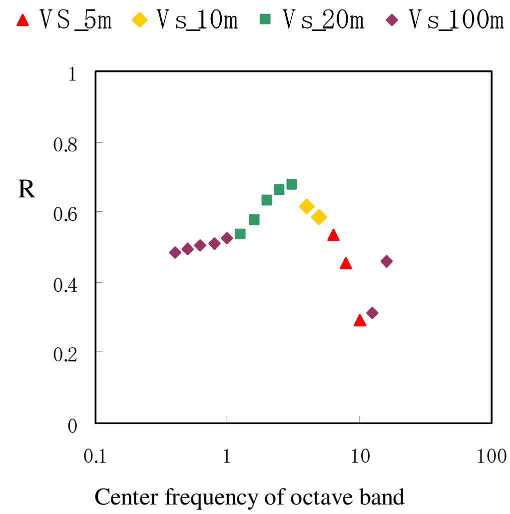

Fig. 24 The best correlation coefficient for each frequency range shown in Fig.23

quency amplification should be controlled by the topmost layers near the surface. However, it is not expected that the highest correlation coefficient is obtained by Vs_20m at around 4 Hz. Fig.24 shows that Vs_10m and Vs_20m are enough to cover a wide range of frequency from 1.25Hz to 5 Hz, which is the most important frequency range for ordinary buildings. For frequencies lower than 1Hz, we need deeper information such as Vs_100m for the best prediction. Note that the best index for frequency bands higher than 10 Hz is also Vs_100m but the correlation is positive. This means that the higher the S-wave velocity in a deeper part, the higher the amplification in these high frequency band. This may come from the fact that high frequency amplification is predominantly caused in a situation with thin soil deposits resting on hard rock and so the level of amplification is determined by S-wave velocity of hard rock, rather than those of soil.

Table 1 Log-linear regression coefficients for spectral site amplification of 1/3 octave bands

Center frequency	Vs_10m	Vs_20m	Vs_30m	Vs_50m	Vs_100m
0.4Hz	$5.6357x^{-0.279}$	$8.1736x^{-0.320}$	$11.656x^{-0.362}$	$18.828x^{-0.414}$	**$29.731x^{-0.455}$**
0.5Hz	$7.6155x^{-0.321}$	$11.791x^{-0.370}$	$18.866x^{-0.427}$	$33.875x^{-0.492}$	**$58.809x^{-0.542}$**
0.63Hz	$9.3684x^{-0.358}$	$15.667x^{-0.417}$	$24.538x^{-0.469}$	$46.669x^{-0.540}$	**$86.497x^{-0.596}$**
0.8Hz	$17.995x^{-0.425}$	$29.221x^{-0.474}$	$46.090x^{-0.525}$	$86.489x^{-0.592}$	**$159.49x^{-0.644}$**
1.0Hz	$35.132x^{-0.486}$	$55.807x^{-0.528}$	$84.195x^{-0.570}$	$142.20x^{-0.619}$	**$239.27x^{-0.657}$**
1.25Hz	$51.108x^{-0.563}$	**$74.939x^{-0.587}$**	$102.20x^{-0.611}$	$148.87x^{-0.636}$	$235.86x^{-0.665}$
1.6Hz	$96.349x^{-0.653}$	**$117.85x^{-0.642}$**	$131.05x^{-0.633}$	$123.85x^{-0.594}$	$139.77x^{-0.578}$
2.0Hz	$258.76x^{-0.779}$	**$320.72x^{-0.762}$**	$343.89x^{-0.742}$	$271.99x^{-0.671}$	$234.35x^{-0.614}$
2.5Hz	$569.23x^{-0.879}$	**$676.64x^{-0.849}$**	$709.83x^{-0.822}$	$530.11x^{-0.739}$	$327.96x^{-0.633}$
3.15Hz	$996.45x^{-0.958}$	**$904.67x^{-0.880}$**	$812.18x^{-0.827}$	$594.59x^{-0.742}$	$293.89x^{-0.604}$
4.0Hz	**$664.42x^{-0.878}$**	$462.19x^{-0.762}$	$366.39x^{-0.695}$	$224.98x^{-0.590}$	$80.527x^{-0.416}$
5.0Hz	**$417.58x^{-0.788}$**	$262.24x^{-0.661}$	$216.48x^{-0.605}$	$127.86x^{-0.499}$	$48.735x^{-0.338}$
6.3Hz	**$158.89x^{-0.631}$**	$81.659x^{-0.483}$	$77.568x^{-0.455}$	$51.983x^{-0.375}$	$22.575x^{-0.239}$
8.0Hz	**$64.884x^{-0.435}$**	$27.052x^{-0.266}$	$26.194x^{-0.250}$	$18.500x^{-0.187}$	$7.5384x^{-0.053}$
10.0Hz	**$24.393x^{-0.252}$**	$10.357x^{-0.098}$	$8.5961x^{-0.065}$	$5.3786x^{0.007}$	$1.7338x^{0.163}$
12.5Hz	$3.4204x^{0.055}$	$2.0386x^{0.135}$	$1.4317x^{0.183}$	$0.8777x^{0.246}$	**$0.2066x^{0.433}$**
16.0Hz	$1.4797x^{0.232}$	$1.2461x^{0.244}$	$0.8605x^{0.291}$	$0.3772x^{0.398}$	**$0.0497x^{0.657}$**

In Table 1 we summarize the log-linear regression coefficient for 1/3-octave-band-averaged spectral site amplifications. Bold face values are those with the highest correlation coefficients as shown in Fig.23. Note that we should limit the amplification level not less than 1.0 even if these equations suggest the values less than 1.0 for high averaged Vs.

CONCLUSIONS

We analyze more than 30,000 strong motion records observed by K-NET, KiK-net, and JMA Shindokei network in Japan and extract source, path, and site effects to characterize statistical nature of moderate and weak ground motions. We found the following:

1) The attenuation in the back-arc region is higher than in the front-arc region as has been reported in literature. The geometrical spreading factor for crustal earthquakes shows distance and frequency dependence, while those for plate boundary and intraplate earthquakes show stable value close to unity.
2) The stress drops of plate boundary and intraplate earthquakes in Japan are 100 bars on the average, while those for crustal earthquakes are only 10 bars. The coefficients of variation are two to three and small depth dependence can be seen. We also see magnitude dependence for those larger than moderate size ($M_0 > 1.0x10^{25}$).
3) The separated spectral site amplifications are found to be very large at certain sites. We successfully invert 1-D S-wave velocity structures based on the separated site amplification factors and PS logging information for K-NET and KiK-net. Based on the total residuals and correlation between theory and observation we select 404 sites where we found good S-wave velocity structures.
4) On the average for these 404 sites site amplification factors are increasing linearly up to 5 until 5 Hz and then become flat until 20 Hz. Their coefficient of variation is 2. We have clear dependence of amplification on the average S-wave velocity up to a certain depth. Among 10 m, 20 m, 30 m, 50 m, and 100 m average, 10 m and 20 m average seem the best choice to represent spectral site amplification in the frequency range important to ordinary buildings. We summarize empirical log-linear relationships with which we can simply estimate spectral amplification based on the averaged S-wave velocity over a certain depth.

By using information presented herein we can evaluate source, path, and site spectra with which we can generate arbitrary numbers of statistical Green's functions for earthquakes with desired sizes, locations, and types. We can use them in quantitative prediction of strong motion for future events. At the same time we can use detailed S-wave velocity structures in a theoretical calculation for lower frequency component of strong motion. Since 404 sites are not enough to cover the whole Japan with sufficient sampling density, we need to invert S-wave velocity structures for the other 1,300 sites with good accuracy. Once we obtain all the site information, then we can quantitatively calculate strong ground motions propagating the whole Japan.

REFERENCES

1. Irikura, K. and K. Kamae, "Physically based source models and strong-ground-motion prediction", *Proceedings of the 11th World Conference on Earthquake Engineering*, Acapulco, June, 1996.
2. Kawase, H., S. Matsushima, R.W. Graves, and P.G. Somerville, "Strong motion simulation of Hyogo-ken Nanbu (Kobe) earthquake considering both the heterogeneous rupture process and the 3-D basin structure", *Proceedings of 12th World Conference on Earthquake Engineering*, Auckland, New Zealand, CD-ROM Ref. No.990, 2000.
3. Graves, R. W., A. Pitarka and P.G. Somerville, "Ground motion amplification in the Santa Monica area: effects of shallow basin edge structure", *Bull. Seismo. Soc. Am*, 88**,** 1224-1242, 1998.

4. Andrews, D.J., "Separation of source and propagation spectra of seven Mammoth Lakes aftershocks", Proc. of Workshop XVI, *Dynamic Characteristic of Faulting*, USGS Open File Report, 1981.
5. Nakamura, R. and T. Uetake, "Three dimensional attenuation structure beneath the Kanto district by using seismic strong motion records, *Zisin*, 2, Vol.56, No.4, 2004 (in press).
6. Fukuyama, M. Ishida, D. Dreger, and H. Kawai, "Automated seismic moment tensor determination by using on-line broadband seismic waveforms", *Zisin,* Vol.51, No.1, 149-156, 1998.
7. Brune J.N., "Tectonic Stress and the Spectra of seismic Shear Waves from Earthquakes", *J. Geophys. Res.*, 75, 4997-5009, 1970.
8. Midorikawa, S., M. Matsuoka, and K. Sakugawa, "Site Effects on Strong-Motion Records during the 1987 Chiba-ken-Toho-Oki, Japan Earthquake", *9^{th} Japan Earthquake Eng. Symp*., Vol.3, 85-90, 1994.
9. Borcherdt, R.D., "Estimates of site-dependent response spectra for design (methodology and justification)", *Earthquake Spectra*, 10, 617- 653, 1994.